

MOX-Report No. 66/2017

**An optimal control problem of two-phase
compressible-incompressible flows**

Tamellini, M.; Parolini, N.; Verani, M.

MOX, Dipartimento di Matematica
Politecnico di Milano, Via Bonardi 9 - 20133 Milano (Italy)

mox-dmat@polimi.it

<http://mox.polimi.it>

An optimal control problem for two-phase compressible-incompressible flows

Mattia Tamellini, Nicola Parolini, Marco Verani
*MOX, Dipartimento di Matematica, Politecnico di Milano,
P.za Leonardo da Vinci 32, I-20133 Milano, Italy*

Abstract

In this work two-phase compressible-incompressible flows are studied. In particular, the possibility of driving the gas bubbles moving in a liquid towards a prescribed position is investigated. To this end, first a well-established mathematical model for two-phase compressible-incompressible fluids is briefly introduced, then an adjoint-based optimal control problem is defined. Finally numerical results on the controllability of the system are presented.

Keywords: optimal control, two-phase compressible-incompressible flows

1. Introduction

Multi-phase flow models describe many phenomena in physics. Indeed, any time two or more fluids move in a given domain they can be represented with a multi-phase model. In compressible-incompressible flow models, one fluid (typically a liquid) is assumed incompressible and interacts with a second fluid (typically a gas) for which compressibility effects cannot be neglected. This class of models is of particular interest for those kinds of applications in which the change of volume of the gaseous component of the multi-phase flow plays a crucial role.

This is the case, for instance, of the production process of metal foams, which are metallic structures containing gaseous inclusions. Gas bubbles are first generated by admixing gas-releasing blowing agents with the molten metal and during the growing process they move within the liquid until the solidification phase starts. The final position and size of such bubbles is what determines the physical properties of the foam. Modelling such a complex process is a challenging task since it involves many different interacting phenomena including fluid-dynamics, chemical reactions, phase-change and heat transfer. We refer to [1] and [2] for an overview on this industrial process and the related modelling

Email addresses: mattia.tamellini@polimi.it (Mattia Tamellini), nicola.parolini@polimi.it (Nicola Parolini), marco.verani@polimi.it (Marco Verani)

approaches. An even tougher challenge is controlling the process by driving the distribution of the gas bubbles towards a desired configuration. The present paper proposes a first contribution in this direction.

The selection of a suitable multi-phase model is critical since it should combine the ability to capture the evolution of compressible bubbles in an incompressible fluid while keeping the overall formulation simple enough to numerically solve an optimal control problem.

When immiscible fluids are considered, different multi-phase models can be devised, each characterised by its own way of keeping track of the region occupied by the different fluids. Limiting our focus to the so-called *front capturing* approaches where the interface position is defined by the value of an auxiliary function, the most common techniques are the *Level Set Method* ([3], [4]), the *Volume Of Fluid Method* ([5]) and the *Ghost Fluid Method* ([6]). Each of these approaches has been widely used in the literature concerning two-phase flows.

In the case of compressible-incompressible flows different models can be adopted for the two fluids. Indeed, while the incompressible fluid is typically modelled by using the incompressible Navier-Stokes equations, the compressible fluid requires a compressible formulation of the flow equations. Therefore, different sets of equations should be solved in the sub-domains occupied by the two phases and, moreover, the position of the interface between these sub-domains is itself an unknown of the problem. When the local fluid-dynamics inside the bubble can be neglected, approximated approaches such as those proposed in [7, 8, 9] can be adopted, where the flow equations (and, in particular, the incompressible Navier-Stokes equations) are solved in the liquid phase, while the gas phase is only characterized by a scalar pressure variable governed by a state equation. In other works, such as for example [10] and [11], the two different sets of equations are solved each in one subdomain, using suitable interface conditions to match the solutions at the interface. This approach, of course, brings along all the issues shared by the problems defined on moving domains (such as fluid-structure interaction problems) and in particular the need to track the interface and to adapt the grid in the sub-domains to always be conforming to the interface itself.

The approach we are interested in uses instead a unified formulation, in which the same set of variables and equations can be used throughout the whole domain. Different models have been proposed in the literature to meet this requirement: a simple unified formulation of the Navier-Stokes equations in terms of primitive unknowns (pressure, velocity, temperature) which is suitable for both compressible and incompressible limits has been proposed in [12] and [13] while in [14] the Low-Mach approximation of the compressible Navier-Stokes equations ([15] and [16]) is used, leading to a more involved model with multiple pressure components. In this work we consider an isothermal version

of the model proposed in [12], also adopted in [17], for which we will derive the optimality conditions required to solve an optimal control problem.

The solution of optimal control problems for compressible-incompressible flows is, to the best of our knowledge, novel in the literature. In general, optimization in the framework of partial differential equations has been investigated for a long time in its various forms, may it be for example inverse problems (see e.g. [18]) or optimal control problems (see e.g. [19] and [20]). More specifically, numerical optimization in the field of computational fluid dynamics has been the object of intensive study, with different goals (e.g. drag reduction, energy minimization, heat dissipation and vorticity reduction). It is beyond the scope of this paper to provide an exhaustive review on the topic. We limit ourselves to recalling, among others, the book [21] and the references therein. In view of the discussion above, the goal of this paper is to provide a first contribution towards the understanding of optimal control problems governed by compressible-incompressible flows.

The outline of the paper is the following. In section 2, the two-phase compressible-incompressible model proposed in [12] and adopted for the problem at hand is briefly recalled. In section 3, an optimal control problem is introduced and the relative optimality conditions are derived. In section 4, the discretization of the primal and adjoint equations and the gradient-type algorithm for the solution of the optimal control problem are introduced. Finally, in section 5, numerical results for the optimal control problems in three relevant test cases are presented and discussed.

2. A mathematical model for two-phase flows

In this section, the model used in this work to describe two-phase compressible-incompressible flows will be introduced. The final goal of the model is to be able to accurately describe the dynamics of a system composed of N gas bubbles contained in a liquid matrix, as shown in figure 1. In particular, we consider the unified formulation proposed in [12], in which the same set of variables is used throughout the whole domain, that is for both the gas and fluid phases.

Let $\Omega \subset \mathbb{R}^d$, $d = 2, 3$, be a sufficiently regular bounded open set. As in [12], [17] and [13], the flow in the liquid phase is governed by the incompressible Navier-Stokes equations

$$\begin{cases} \nabla \cdot \mathbf{u} = 0, \\ \rho \frac{\partial \mathbf{u}}{\partial t} + \rho (\mathbf{u} \cdot \nabla) \mathbf{u} - \nabla \cdot \boldsymbol{\tau} + \nabla p = \rho \mathbf{g}, \end{cases} \quad (1)$$

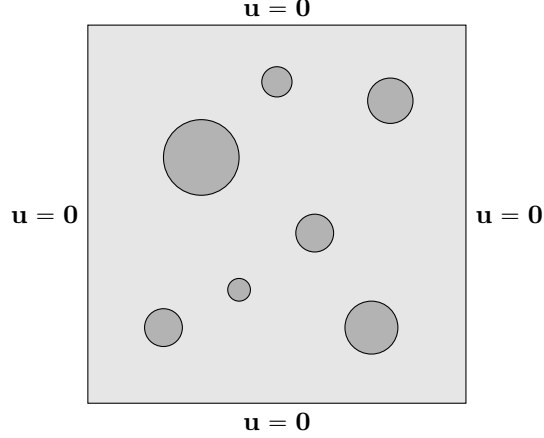


Figure 1: Example setting for the physical system of interest. In dark grey the gas bubbles and in lighter grey the liquid matrix

while in the gaseous phase the compressible isothermal Navier-Stokes equations

$$\begin{cases} \frac{\partial \rho}{\partial t} + \nabla \cdot (\rho \mathbf{u}) = 0, \\ \rho \frac{\partial \mathbf{u}}{\partial t} + \rho (\mathbf{u} \cdot \nabla) \mathbf{u} - \nabla \cdot \boldsymbol{\tau} + \nabla p = \rho \mathbf{g}, \\ p = \rho r T \end{cases} \quad (2)$$

are considered, where the gas is assumed to be perfect. In the above systems, $\mathbf{u} = \mathbf{u}(\mathbf{x}, t)$ denotes the velocity, $p = p(\mathbf{x}, t)$ the pressure, $\rho = \rho(\mathbf{x}, t)$ the density, the temperature T is assumed to be constant both in space and in time, r is the specific gas constant and \mathbf{g} the gravitational acceleration. Both systems must then be closed by suitable initial and boundary conditions.

In this work, fluids are all supposed to be Newtonian, so the viscous stress tensor is given by the constitutive equation

$$\boldsymbol{\tau} = \lambda (\nabla \cdot \mathbf{u}) \mathbf{I} + 2\mu \mathbf{D},$$

where $\mu = \mu(\mathbf{x}, t)$ represents the viscosity, $\lambda = \lambda(\mathbf{x}, t)$ is the second viscosity coefficient (in general, $\lambda = -2/3\mu$) and

$$\mathbf{D} = \frac{\nabla \mathbf{u} + (\nabla \mathbf{u})^t}{2}.$$

To write a single, unified formulation, valid in the whole domain Ω and which uses the same set of variables in both phases, following [12], a Level Set approach was used, tracking the interface between the two phases as the zero level-set of a signed distance function $\varphi(\mathbf{x}, t)$. This function will then be

used to compute the Heaviside function:

$$H(\mathbf{x}, t) = \begin{cases} 1 & \text{in the gas } (\varphi \leq 0), \\ 0 & \text{in the liquid } (\varphi > 0), \end{cases}$$

which in turn will be employed to define the physical properties ρ , μ , λ and χ_T in the whole domain by mixing the corresponding properties of each single phase. For each quantity, we will use subscripts l and g to indicate “liquid” and “gas”, respectively.

In view of the above discussion, the two-phase model stemming from (1) and (2) reads as follows:

$$\left\{ \begin{array}{ll} \nabla \cdot \mathbf{u} + \chi_T \left(\frac{\partial p}{\partial t} + \mathbf{u} \cdot \nabla p \right) = 0 & \text{in } \Omega \times (t_0, t_f], \\ \rho \frac{\partial \mathbf{u}}{\partial t} + \rho (\mathbf{u} \cdot \nabla) \mathbf{u} - \nabla \cdot \boldsymbol{\tau} + \nabla p = \rho \mathbf{g} + \mathbf{s} & \text{in } \Omega \times (t_0, t_f], \\ \frac{\partial \varphi}{\partial t} + \mathbf{u} \cdot \nabla \varphi = 0 & \text{in } \Omega \times (t_0, t_f], \\ H = H(\varphi) = \begin{cases} 1 & \text{if } \varphi \leq 0 \\ 0 & \text{if } \varphi > 0 \end{cases} & \text{in } \Omega \times (t_0, t_f], \\ \rho = \frac{p}{rT} H + \rho_l (1 - H) & \text{in } \Omega \times (t_0, t_f], \\ \mu = \mu_g H + \mu_l (1 - H) & \text{in } \Omega \times (t_0, t_f], \\ \lambda = \lambda_g H + \lambda_l (1 - H) & \text{in } \Omega \times (t_0, t_f], \\ \chi_T = \frac{1}{p} H & \text{in } \Omega \times (t_0, t_f], \\ \text{boundary conditions} & \text{on } \partial\Omega \times (t_0, t_f], \\ \text{initial conditions} & \text{in } \Omega, \end{array} \right. \quad (3)$$

where ρ_l , μ_g , μ_l , λ_g and λ_l are given constants depending on the fluids and χ_T denotes the *isothermal compressibility*. See [12] for further details.

Notice that the different values of λ and μ in the two phases also enter in the definitions of the viscous stress tensor $\boldsymbol{\tau}$. Moreover, in the incompressible case, since $\nabla \cdot \mathbf{u} = 0$, the viscous stress tensor reverts back to the standard incompressible constitutive equation:

$$\boldsymbol{\tau} = 2\mu \mathbf{D}.$$

Notice also that the surface tension term

$$\mathbf{s}(\mathbf{x}, t) = \varsigma \kappa \mathbf{n} \quad \forall (\mathbf{x}, t) \in \Sigma(t)$$

was added to the right hand side of the momentum equation, where $\Sigma = \Sigma(t)$ denotes the interface between the two phases, being ς a constant representing the surface tension coefficient, \mathbf{n} the normal

vector to the interface and κ the curvature. As it is classical in the level set method, we have the following relations:

$$\begin{aligned}\mathbf{n} &= \frac{\nabla\varphi}{\|\nabla\varphi\|}, \\ \kappa &= -\nabla \cdot \mathbf{n} = -\nabla \cdot \frac{\nabla\varphi}{\|\nabla\varphi\|}.\end{aligned}\tag{4}$$

The surface tension term $\mathbf{s}(\mathbf{x}, t)$ can be equivalently defined on the whole domain Ω as:

$$\mathbf{s}(\mathbf{x}, t) = \varsigma \kappa \mathbf{n} \delta(\Sigma),$$

where $\delta(\Sigma)$ is the Dirac function associated with Σ . See [22] for further details.

To reduce the onset of numerical instabilities of the discrete solution at the interface, the function $H(\varphi)$ will be substituted by a smoothed approximation, which reads:

$$H_\varepsilon(x) = \begin{cases} 1 & \text{if } x < -\frac{\varepsilon}{2}, \\ \frac{1}{2} \left(1 + \cos\left(\pi \frac{2x + \varepsilon}{2\varepsilon}\right) \right) & \text{if } -\frac{\varepsilon}{2} \leq x \leq \frac{\varepsilon}{2}, \\ 0 & \text{if } x > \frac{\varepsilon}{2}, \end{cases}\tag{5}$$

for a given a constant $\varepsilon \in \mathbb{R}^+$. Similarly, the Dirac function will be replaced by a smoothed approximation, namely

$$\delta_\varepsilon(x) = \frac{dF_\varepsilon}{dx} = \begin{cases} 0 & \text{if } x < -\frac{\varepsilon}{2}, \\ -\frac{1}{2} \frac{\pi}{\varepsilon} \sin\left(\pi \frac{2x + \varepsilon}{2\varepsilon}\right) & \text{if } -\frac{\varepsilon}{2} \leq x \leq \frac{\varepsilon}{2}, \\ 0 & \text{if } x > \frac{\varepsilon}{2}. \end{cases}\tag{6}$$

Finally, we remark that in model (3) the two phases are immiscible and no mass transfer at the interface is considered.

3. An optimal control problem

Let Ω represent a box containing a given number of gas bubbles moving within a liquid. Our aim is to formulate an optimal control problem whose solution yields the volumetric force to be applied to the system in order to drive the gas bubbles to a given final position at a given time. An example setting is shown in figure 2.

Let us denote by \mathbf{C} the control variable acting on the right hand side of the momentum equation.

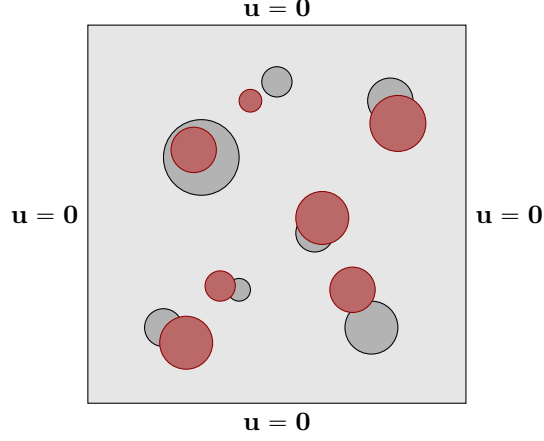


Figure 2: Example setting for the optimal control problem of interest. In red the target position for the evolution of the bubbles and in dark grey a possible distribution of the bubbles at the final time t_f in the uncontrolled case.

Then the state system reads as follows:

$$\left\{ \begin{array}{ll}
 \nabla \cdot \mathbf{u} + \chi_T \left(\frac{\partial p}{\partial t} + \mathbf{u} \cdot \nabla p \right) = 0 & \text{in } \Omega \times (t_0, t_f], \\
 \rho \frac{\partial \mathbf{u}}{\partial t} + \rho (\mathbf{u} \cdot \nabla) \mathbf{u} - \nabla \cdot \boldsymbol{\tau} + \nabla p = \rho \mathbf{g} + \rho \mathbf{C} + \mathbf{s} & \text{in } \Omega \times (t_0, t_f], \\
 \frac{\partial \varphi}{\partial t} + \mathbf{u} \cdot \nabla \varphi = 0 & \text{in } \Omega \times (t_0, t_f], \\
 H = F(\varphi) = \begin{cases} 1 & \text{if } \varphi \leq 0 \\ 0 & \text{if } \varphi > 0 \end{cases} & \text{in } \Omega \times (t_0, t_f], \\
 \rho = \frac{p}{rT} H + \rho_l (1 - H) & \text{in } \Omega \times (t_0, t_f], \\
 \mu = \mu_g H + \mu_l (1 - H) & \text{in } \Omega \times (t_0, t_f], \\
 \lambda = \lambda_g H + \lambda_l (1 - H) & \text{in } \Omega \times (t_0, t_f], \\
 \chi_T = \frac{1}{p} H & \text{in } \Omega \times (t_0, t_f], \\
 \mathbf{u} = \mathbf{0} & \text{on } \partial\Omega \times (t_0, t_f], \\
 \mathbf{u}|_{t=t_0} = \mathbf{u}_0 & \text{in } \Omega, \\
 \varphi|_{t=t_0} = \varphi_0 & \text{in } \Omega,
 \end{array} \right. \quad (7)$$

where, for simplicity, we enforced homogeneous Dirichlet boundary conditions for the velocity.

We are interested in solving the following minimization problem:

Problem 1. Let $\mathcal{C} = L^2 \left((t_0, t_f); (H^1(\Omega))^d \right)$ be the space of admissible controls. Given two constants $\sigma_1, \sigma_2 \in \mathbb{R}$, a function $\bar{\varphi}: \Omega \rightarrow \mathbb{R}$ and an objective functional J defined as:

$$\begin{aligned} J: \mathcal{C} &\rightarrow \mathbb{R} \\ C &\rightarrow J(\mathbf{C}) = \frac{\sigma_1}{2} \int_{\Omega} \left(\varphi(\mathbf{C})|_{t=t_f} - \bar{\varphi} \right)^2 dx + \frac{\sigma_2}{2} \|\mathbf{C}\|_{\mathcal{C}}^2, \end{aligned} \quad (8)$$

find $\mathbf{C}^* = \operatorname{argmin}_{\mathbf{C} \in \mathcal{C}} J(\mathbf{C})$ such that the equation system (7) holds.

Let us comment on the objective functional (8). The first term ensures that the final solution for the signed distance equation (7)₃ is close to the target solution $\bar{\varphi}$. This amounts to prescribing a final distribution of the bubbles. The second term is a standard term penalising the norm of the control.

In view of designing a numerical algorithm to solve problem 1, the following result will be crucial.

Theorem 1 (Optimality conditions). *The optimality conditions for the two-phase compressible-incompressible control problem 1 are given by:*

i) the state system (7)

ii) the adjoint system

$$\left\{ \begin{array}{ll} -\frac{\partial}{\partial t}(\rho \hat{\mathbf{u}}) + \rho(\nabla \mathbf{u})^T \cdot \hat{\mathbf{u}} - \rho(\mathbf{u} \cdot \nabla) \hat{\mathbf{u}} - \nabla \cdot (\mu \nabla \hat{\mathbf{u}} + \mu(\nabla \hat{\mathbf{u}})^t) + & \text{in } \Omega \times (t_0, t_f], \\ -\nabla(\lambda \nabla \cdot \hat{\mathbf{u}}) - \nabla \hat{p} + \chi_T \hat{p} \nabla p + \nabla \varphi \hat{\varphi} = 0 & \\ \nabla \cdot \hat{\mathbf{u}} = -\frac{\partial}{\partial t}(\chi_T \hat{p}) - \nabla \cdot (\chi_T \mathbf{u} \hat{p}) + \frac{H}{rT} \hat{p} + \chi_T \hat{\chi}_T & \text{in } \Omega \times (t_0, t_f], \\ -\frac{\partial \hat{\varphi}}{\partial t} - \nabla \cdot (\hat{\varphi} \mathbf{u}) = -\delta^*(\varphi) \hat{H} + R(\varphi, \hat{\mathbf{u}}) & \text{in } \Omega \times (t_0, t_f], \\ \hat{H} = \left(\frac{p}{rT} - \rho_l \right) \hat{p} + (\mu_g - \mu_l) \hat{\mu} + & \text{in } \Omega \times (t_0, t_f], \\ \quad + (\lambda_g - \lambda_l) \hat{\lambda} + \hat{\chi}_T & \\ \hat{p} = -\frac{\partial \mathbf{u}}{\partial t} \cdot \hat{\mathbf{u}} - (\mathbf{u} \cdot \nabla) \mathbf{u} \cdot \hat{\mathbf{u}} + \mathbf{g} \cdot \hat{\mathbf{u}} + \mathbf{C} \cdot \hat{\mathbf{u}} & \text{in } \Omega \times (t_0, t_f], \\ \hat{\mu} = -\nabla \mathbf{u} : \nabla \hat{\mathbf{u}} - (\nabla \mathbf{u})^t : \nabla \hat{\mathbf{u}} & \text{in } \Omega \times (t_0, t_f], \\ \hat{\lambda} = -((\nabla \cdot \mathbf{u}) \mathbf{I}) : \nabla \hat{\mathbf{u}} & \text{in } \Omega \times (t_0, t_f], \\ p \hat{\chi}_T = -\hat{p} \left(\frac{\partial p}{\partial t} + \mathbf{u} \cdot \nabla p \right) & \text{in } \Omega \times (t_0, t_f], \\ \hat{\mathbf{u}} = \mathbf{0} & \text{on } \partial \Omega, \\ \hat{\mathbf{u}}|_{t=t_f} = \mathbf{0} & \text{in } \Omega, \\ \hat{p}|_{t=t_f} = 0 & \text{in } \Omega, \\ \hat{\varphi}|_{t=t_f} = \sigma_1 \left(\varphi|_{t=t_f} - \bar{\varphi} \right) & \text{in } \Omega, \end{array} \right. \quad (9)$$

where $\hat{\mathbf{u}}, \hat{p}, \hat{\varphi}, \hat{H}, \hat{\rho}, \hat{\mu}, \hat{\lambda}$ and $\hat{\chi}_T$ are the so-called adjoint variables. The source term $R(\varphi, \hat{\mathbf{u}})$ in equation (9)₃ is defined as:

$$R(\varphi, \hat{\mathbf{u}}) = \nabla \cdot \left(\left(-\nabla \left(\varsigma \frac{\nabla \varphi}{\|\nabla \varphi\|} \delta_\varepsilon(\varphi) \hat{\mathbf{u}} \right) + \varsigma \nabla \cdot \left(\frac{\nabla \varphi}{\|\nabla \varphi\|} \right) \delta_\varepsilon(\varphi) \hat{\mathbf{u}} \right) \frac{1}{\|\nabla \varphi\|} \left(1 - \left(\frac{\nabla \varphi}{\|\nabla \varphi\|} \right)^2 \right) \right) + \nabla \cdot \left(\frac{\nabla \varphi}{\|\nabla \varphi\|} \right) \frac{\nabla \varphi}{\|\nabla \varphi\|} \delta'_\varepsilon(\varphi) \hat{\mathbf{u}},$$

where $\delta'_\varepsilon(\varphi)$ denotes the derivative of the smooth Dirac's delta function (6).

iii) the variational equality

$$\sigma_2 (\mathbf{C}, \delta \mathbf{C})_{\mathcal{C}} + \int_{t_0}^{t_f} \int_{\Omega} \rho \delta \mathbf{C} \cdot \hat{\mathbf{u}} \, d\mathbf{x} \, dt = 0 \quad \forall \delta \mathbf{C} \in \mathcal{C}, \quad (10)$$

where $(\cdot, \cdot)_{\mathcal{C}}$ denotes the usual scalar product in $L^2 \left((t_0, t_f); (H^1(\Omega))^d \right)$.

Proof. Denoting by $\mathbf{y} = (\mathbf{u}, p, \varphi, H, \rho, \mu, \lambda, \chi_T)$ and by $\hat{\mathbf{y}} = (\hat{\mathbf{u}}, \hat{p}, \hat{\varphi}, \hat{H}, \hat{\rho}, \hat{\mu}, \hat{\lambda}, \hat{\chi}_T)$ the state and adjoint variables, respectively, we consider the following Lagrangian functional:

$$\begin{aligned} \mathcal{L}(\mathbf{y}, \hat{\mathbf{y}}, \mathbf{C}) &= \frac{\sigma_1}{2} \int_{\Omega} \left(\varphi(\mathbf{C})|_{t=t_f} - \bar{\varphi} \right)^2 \, d\mathbf{x} + \frac{\sigma_2}{2} \|\mathbf{C}\|_{\mathcal{C}}^2 + \\ &- \int_{t_0}^{t_f} \int_{\Omega} \left(\rho \frac{\partial \mathbf{u}}{\partial t} + \rho (\mathbf{u} \cdot \nabla) \mathbf{u} - \nabla \cdot \left(\mu \nabla \mathbf{u} + \mu (\nabla \mathbf{u})^t + \lambda (\nabla \cdot \mathbf{u}) \mathbf{I} \right) + \nabla p - \rho \mathbf{g} - \rho \mathbf{C} - \mathbf{s} \right) \cdot \hat{\mathbf{u}} \, d\mathbf{x} \, dt + \\ &- \int_{t_0}^{t_f} \int_{\Omega} \left(\nabla \cdot \mathbf{u} + \chi_T \left(\frac{\partial p}{\partial t} + \mathbf{u} \cdot \nabla p \right) \right) \hat{p} \, d\mathbf{x} \, dt - \int_{t_0}^{t_f} \int_{\Omega} \left(\frac{\partial \varphi}{\partial t} + \mathbf{u} \cdot \nabla \varphi \right) \hat{\varphi} \, d\mathbf{x} \, dt + \\ &- \int_{t_0}^{t_f} \int_{\Omega} (H - F(\varphi)) \hat{H} \, d\mathbf{x} \, dt - \int_{t_0}^{t_f} \int_{\Omega} \left(\rho - \frac{p}{rT} H - (1 - H) \rho_l \right) \hat{\rho} \, d\mathbf{x} \, dt + \\ &- \int_{t_0}^{t_f} \int_{\Omega} (\mu - \mu_g H - (1 - H) \mu_l) \hat{\mu} \, d\mathbf{x} \, dt - \int_{t_0}^{t_f} \int_{\Omega} (\lambda - \lambda_g H - (1 - H) \lambda_l) \hat{\lambda} \, d\mathbf{x} \, dt + \\ &- \int_{t_0}^{t_f} \int_{\Omega} (p \chi_T - H) \hat{\chi}_T \, d\mathbf{x} \, dt - \int_{t_0}^{t_f} \int_{\partial \Omega} \mathbf{u} \cdot \hat{\boldsymbol{\theta}}_1 \, ds \, dt - \int_{\Omega} (\mathbf{u}|_{t=t_0} - \mathbf{u}_0) \cdot \hat{\boldsymbol{\theta}}_2 \, d\mathbf{x} + \\ &- \int_{\Omega} (\varphi|_{t=t_0} - \varphi_0) \hat{\theta}_3 \, d\mathbf{x}. \end{aligned} \quad (11)$$

The first term on the right hand side of (11) is the cost functional J , while the remaining terms are the inner products between the equations in the state system and the adjoint variables, which assume the role of Lagrangian multipliers.

The thesis is obtained by looking for a stationary point of \mathcal{L} , i.e.

$$\nabla \mathcal{L} = \mathbf{0}.$$

Indeed, as it is standard in the optimal control problems via Lagrangian approach (see e.g. [20]), by computing the derivatives of \mathcal{L} with respect to the adjoint variables and by setting them all equal

to zero, we recover the state system (7). On the other hand, by computing the derivatives of \mathcal{L} with respect to the primal variables, we obtain the adjoint system (9). Finally, by deriving the lagrangian functional with respect to the control variable \mathbf{C} , we obtain the variational equality (10). Further details can be found in [23]. \square

It is important to remark (see [20]) that the variational equality (10) yields the gradient of the cost functional with respect to the control variable. Indeed, (10) can be rewritten as:

$$(\nabla_{\mathbf{C}} J, \delta \mathbf{C})_{\mathcal{C}} = 0 \quad \forall \delta \mathbf{C} \in \mathcal{C},$$

with

$$\nabla_{\mathbf{C}} J = \sigma_2 \mathbf{C} + \rho \hat{\mathbf{u}}. \quad (12)$$

The gradient equation (12) will be employed to design a gradient-type algorithm, which will be detailed in section 4.

4. Space-time discretization and minimization algorithm

The systems described in sections 2 and 3 have been approximated by using a Finite Element discretization in space, while a Finite Difference approach was used for the time discretization. To this end, the solution interval $(t_0, t_f]$ is divided into N subintervals of length $\Delta t = \frac{t_f - t_0}{N}$. In the following, a superscript (n) will denote the value of each quantity at time $t^{(n)} = t_0 + n \Delta t$. As for the space discretization at each timestep $t^{(n)}$, for $(\mathbf{u}^{(n)}, p^{(n)})$ and $(\hat{\mathbf{u}}^{(n)}, \hat{p}^{(n)})$ we use continuous $\mathbb{P}_2/\mathbb{P}_1$ finite elements, which are inf-sup stable (see e.g. [24]); for $\varphi^{(n)}$ and $\hat{\varphi}^{(n)}$ we choose discontinuous \mathbb{P}_1 finite elements, following the discretization for the level set equation adopted in [25]; finally, continuous \mathbb{P}_1 finite elements are used for all the remaining primal and adjoint quantities, including the control variable \mathbf{C} . For each continuous quantity, a subscript h will denote its discrete counterpart.

The result of the space-time discretization is a non-linear system of equations that needs to be solved at each timestep. As a monolithic approach would be computationally unfeasible given the complexity of the system, we employ a staggered approach to define a sequence of simpler problems to be solved at each time step.

Let us introduce some preliminary notation that will be used throughout the remainder of the section. Let \mathcal{T}_h be the triangulation on the domain Ω and let $\{E_i\}$ be the elements of \mathcal{T}_h . We

consider the following discrete functional spaces:

$$\begin{aligned} V_h &= \{v_h \in C^0(\Omega) : v_h|_E \in \mathbb{P}^2 \ \forall E \in \mathcal{T}_h\}, \\ Q_h &= \{q_h \in C^0(\Omega) : q_h|_E \in \mathbb{P}^1 \ \forall E \in \mathcal{T}_h\}, \\ W_h &= \{w_h \in L^2(\Omega) : w_h|_E \in \mathbb{P}^1 \ \forall E \in \mathcal{T}_h\}. \end{aligned}$$

Consider then an edge e of $E_i \in \mathcal{T}_h$. Given generic scalar-valued and vector-valued functions f and \mathbf{F} , let f_i and \mathbf{F}_i denote the traces of f and \mathbf{F} on e as taken in E_i , respectively, and let $\boldsymbol{\nu}_i$ be the outward normal vector on e with respect to E_i . If e is an internal edge shared by elements E_i and E_j , we define:

$$\begin{aligned} \llbracket f \rrbracket &:= f_i \boldsymbol{\nu}_i + f_j \boldsymbol{\nu}_j, & \{f\} &:= \frac{1}{2} (f_i + f_j), \\ \llbracket \mathbf{F} \rrbracket &:= \mathbf{F}_i \cdot \boldsymbol{\nu}_i + \mathbf{F}_j \cdot \boldsymbol{\nu}_j, & \{\mathbf{F}\} &:= \frac{1}{2} (\mathbf{F}_i + \mathbf{F}_j). \end{aligned}$$

For a boundary edge e , on the other hand, we define:

$$\llbracket f \rrbracket := f_i \boldsymbol{\nu}_i, \quad \{f\} := f_i.$$

Finally, we will denote by \mathcal{E}_0 the set of all internal edges and \mathcal{E}_∂ the set of all boundary edges.

Let us now describe the staggered approach used to solve system (7). Given the initial conditions $\varphi_h^{(0)}$, $\mathbf{u}_h^{(0)}$, $p_h^{(0)}$, $\rho_h^{(0)}$, $\mu_h^{(0)}$, $\lambda_h^{(0)}$, and $\chi_{T_h}^{(0)}$, for every $n = 1, 2, \dots, N$, the solution process is as follows:

1P. Compute $\mathbf{u}_h^{(n)}$ and $p_h^{(n)}$, by solving the following discrete problem:

Find $(\mathbf{u}_h^{(n)}, p_h^{(n)})$ in $V_h^d \times Q_h$ such that

$$\begin{aligned} & \int_{\Omega} \frac{\rho_h^{(n-1)}}{\Delta t} \mathbf{u}_h^{(n)} \cdot \mathbf{v}_h \, d\mathbf{x} + \int_{\Omega} \rho_h^{(n-1)} (\mathbf{u}_h^{(n-1)} \cdot \nabla) \mathbf{u}_h^{(n)} \cdot \mathbf{v}_h \, d\mathbf{x} + \int_{\Omega} \boldsymbol{\tau}_h^{(n)} \cdot \nabla \mathbf{v}_h \, d\mathbf{x} + \\ & - \int_{\Omega} p_h^{(n)} \nabla \cdot \mathbf{v}_h \, d\mathbf{x} + \int_{\Omega} \nabla \cdot \mathbf{u}_h^{(n)} q_h \, d\mathbf{x} + \int_{\Omega} \frac{\chi_{T_h}^{(n-1)}}{\Delta t} p_h^{(n)} q_h \, d\mathbf{x} + \int_{\Omega} \chi_{T_h}^{(n-1)} \mathbf{u}_h^{(n-1)} \cdot \nabla p_h^{(n)} q_h \, d\mathbf{x} = \\ & = \int_{\Omega} \frac{\rho_h^{(n-1)}}{\Delta t} \mathbf{u}_h^{(n-1)} \cdot \mathbf{v}_h \, d\mathbf{x} + \int_{\Omega} \rho_h^{(n-1)} \mathbf{g} \cdot \mathbf{v}_h \, d\mathbf{x} + \int_{\Omega} \mathbf{s}_h^{(n-1)} \cdot \mathbf{v}_h \, d\mathbf{x} + \int_{\Omega} \frac{\chi_{T_h}^{(n-1)}}{\Delta t} p_h^{(n-1)} q_h \, d\mathbf{x} + \\ & + \int_{\Omega} \mathbf{C}_h^{(n)} q_h \, d\mathbf{x} \quad \forall (\mathbf{v}_h, q_h) \in V_h^d \times Q_h, \end{aligned}$$

where

$$\boldsymbol{\tau}_h^{(n)} = \lambda_h^{(n-1)} (\nabla \cdot \mathbf{u}_h^{(n)}) \mathbf{I} + 2\mu_h^{(n-1)} \frac{\nabla \mathbf{u}_h^{(n)} + (\nabla \mathbf{u}_h^{(n)})^t}{2}$$

and

$$\mathbf{s}_h^{(n-1)} = \varsigma \kappa_h^{(n-1)} \mathbf{n}_h^{(n-1)} \delta_\varepsilon (\Sigma_h^{(n-1)}),$$

with $\kappa_h^{(n-1)}$ and $\mathbf{n}_h^{(n-1)}$ computed using (4).

2P. Compute the signed distance function $\varphi_h^{(n)}$, by solving the following discrete level-set equation:

Find $\varphi_h^{(n)}$ in W_h such that

$$\begin{aligned} & \sum_{E \in \mathcal{T}_h} \int_E \frac{\varphi_h^{(n)}}{\Delta t} w_h \, d\mathbf{x} - \sum_{E \in \mathcal{T}_h} \int_E \varphi_h^{(n)} \mathbf{u}_h^{(n)} \cdot \nabla w_h \, d\mathbf{x} - \sum_{E \in \mathcal{T}_h} \int_E \varphi_h^{(n)} \nabla \cdot \mathbf{u}_h^{(n)} w_h \, d\mathbf{x} + \\ & + \sum_{e \in \mathcal{E}_\rho} \int_e \mathbf{u}_h^{(n)} \cdot \llbracket w_h \rrbracket \left\{ \varphi_h^{(n)} \right\} \, ds + \sum_{e \in \mathcal{E}_0} \int_e \left(\left\{ \varphi_h^{(n)} \right\} \mathbf{u}_h^{(n)} \llbracket w_h \rrbracket + \frac{1}{2} \left| \mathbf{u}_h^{(n)} \cdot \boldsymbol{\nu} \right| \llbracket \varphi_h^{(n)} \rrbracket \cdot \llbracket w_h \rrbracket \right) \, ds = \\ & = \sum_{E \in \mathcal{T}_h} \int_E \frac{\varphi_h^{(n-1)}}{\Delta t} w_h \, d\mathbf{x} \quad \forall w_h \in W_h. \end{aligned}$$

See [25] for more details.

3P. Compute $H_h^{(n)}$, using the smoothed approximation (5).

4P. Update the physical parameters $\rho_h^{(n)}$, $\mu_h^{(n)}$, $\lambda_h^{(n)}$, $\chi_{T_h}^{(n)}$ using equations (7)₅, (7)₆, (7)₇ and (7)₈, respectively.

5P. If $n < N$, set $n = n + 1$ and go back to 1P.

Concerning the adjoint system (9), notice that, as it is classical, it is a backwards-in-time problem (with a structure similar to the one of the primal problem). Given the final conditions $\hat{\varphi}_h^{(N)}$, $\hat{\mathbf{u}}_h^{(N)}$, $\hat{p}_h^{(N)}$, $\hat{\rho}_h^{(N)}$, $\hat{\mu}_h^{(N)}$, $\hat{\lambda}_h^{(N)}$, and $\hat{\chi}_{T_h}^{(N)}$, for every $n = N - 1, N - 2, \dots, 0$, the solution process is as follows:

1A. Compute $\hat{\mathbf{u}}_h^{(n)}$ and $\hat{p}_h^{(n)}$, solving the following discrete problem:

Find $(\hat{\mathbf{u}}_h^{(n)}, \hat{p}_h^{(n)})$ in $V_h^d \times Q_h$ such that

$$\begin{aligned} & \int_{\Omega} \frac{\rho_h^{(n)}}{\Delta t} \hat{\mathbf{u}}_h^{(n)} \cdot \mathbf{v}_h \, d\mathbf{x} + \int_{\Omega} \rho_h^{(n)} \left(\nabla \mathbf{u}_h^{(n)} \right)^t \cdot \hat{\mathbf{u}}_h^{(n)} \cdot \mathbf{v}_h \, d\mathbf{x} - \int_{\Omega} \rho_h^{(n)} \left(\mathbf{u}_h^{(n)} \cdot \nabla \right) \hat{\mathbf{u}}_h^{(n)} \cdot \mathbf{v}_h \, d\mathbf{x} + \\ & + \int_{\Omega} \mu_h^{(n)} \nabla \hat{\mathbf{u}}_h^{(n)} : \nabla \mathbf{v}_h \, d\mathbf{x} + \int_{\Omega} \mu_h^{(n)} \left(\nabla \hat{\mathbf{u}}_h^{(n)} \right)^t : \nabla \mathbf{v}_h \, d\mathbf{x} + \int_{\Omega} \lambda_h^{(n)} \nabla \cdot \hat{\mathbf{u}}_h^{(n)} \nabla \cdot \mathbf{v}_h \, d\mathbf{x} + \\ & + \int_{\Omega} \hat{p}_h^{(n)} \nabla \cdot \mathbf{v}_h \, d\mathbf{x} + \int_{\Omega} \chi_{T_h}^{(n)} \hat{p}_h^{(n)} \nabla p_h^{(n)} \cdot \mathbf{v}_h \, d\mathbf{x} + \int_{\Omega} \nabla \cdot \hat{\mathbf{u}}_h^{(n)} q_h \, d\mathbf{x} - \int_{\Omega} \frac{\chi_{T_h}^{(n)}}{\Delta t} \hat{p}_h^{(n)} q_h \, d\mathbf{x} + \\ & + \int_{\Omega} \nabla \cdot \left(\chi_{T_h}^{(n)} \mathbf{u}_h^{(n)} \hat{p}_h^{(n)} \right) q_h \, d\mathbf{x} = \int_{\Omega} \frac{\rho_h^{(n+1)}}{\Delta t} \hat{\mathbf{u}}_h^{(n+1)} \cdot \mathbf{v}_h \, d\mathbf{x} - \int_{\Omega} \frac{\chi_{T_h}^{(n+1)}}{\Delta t} \hat{p}_h^{(n+1)} q_h \, d\mathbf{x} + \\ & - \int_{\Omega} \hat{\varphi}_h^{(n+1)} \nabla \varphi_h^{(n)} \cdot \mathbf{v}_h \, d\mathbf{x} + \int_{\Omega} \frac{H_h^{(n)}}{rT} \hat{\rho}_h^{(n+1)} q_h \, d\mathbf{x} + \int_{\Omega} \chi_{T_h}^{(n)} \hat{\chi}_{T_h}^{(n+1)} \, d\mathbf{x} \quad \forall (\mathbf{v}_h, q_h) \in V_h^d \times Q_h. \end{aligned}$$

2A. Compute the adjoint signed distance function $\hat{\varphi}_h^{(n)}$, solving the following discrete problem:

Find $\hat{\varphi}_h^{(n)}$ in W_h such that

$$\begin{aligned} & \sum_{E \in \mathcal{T}_h} \int_E \frac{\hat{\varphi}_h^{(n)}}{\Delta t} w_h \, d\mathbf{x} - \sum_{E \in \mathcal{T}_h} \int_E \hat{\varphi}_h^{(n)} \mathbf{u}_h^{(n)} \cdot \nabla w_h \, d\mathbf{x} + \sum_{e \in \mathcal{E}_\partial} \int_e \mathbf{u}_h^{(n)} \cdot \llbracket w_h \rrbracket \left\{ \hat{\varphi}_h^{(n)} \right\} \, ds + \\ & + \sum_{e \in \mathcal{E}_0} \int_e \left(\left\{ \hat{\varphi}_h^{(n)} \right\} \mathbf{u}_h^{(n)} \llbracket w_h \rrbracket + \frac{1}{2} \left| \mathbf{u}_h^{(n)} \cdot \boldsymbol{\nu} \right| \llbracket \hat{\varphi}_h^{(n)} \rrbracket \cdot \llbracket w_h \rrbracket \right) \, ds = \sum_{E \in \mathcal{T}_h} \int_E \frac{\hat{\varphi}_h^{(n+1)}}{\Delta t} w_h \, d\mathbf{x} + \\ & + \sum_{E \in \mathcal{T}_h} \int_E \left(\delta_\varepsilon \left(\varphi_h^{(n)} \right) + R \left(\varphi_h^{(n)}, \hat{\mathbf{u}}_h^{(n)} \right) \right) w_h \, d\mathbf{x} \quad \forall w_h \in W_h. \end{aligned}$$

3A. Compute $\hat{H}_h^{(n)}$ using equation (9)₄.

4A. Update the adjoint physical parameters $\hat{\rho}_h^{(n)}$, $\hat{\mu}_h^{(n)}$, $\hat{\lambda}_h^{(n)}$, $\hat{\chi}_{T_h}^{(n)}$ using equations (9)₅, (9)₆, (9)₇ and (9)₈, respectively.

5A. If $n < N$, set $n = n + 1$ and go back to 1A.

As mentioned above, the optimal control problem is solved using an iterative algorithm to get to the minimum of the cost functional. In particular, the descent direction at the k -th minimization step, denoted by \mathbf{d} , is chosen using a *gradient method*, which means:

$$\mathbf{d} = -\nabla J \left(\mathbf{C}^{(k)} \right),$$

where $\mathbf{C}^{(k)}$ is the value of the control variable at the k -th iteration in the minimization loop. On the other hand, the length of the step along the selected direction, which will be denoted by α , is computed with a *backtracking algorithm*. The best approach in terms of speed of convergence would of course be to move along the direction given by the gradient of the cost functional until the minimum value on that line is reached. However, the solution of this mono-dimensional exact minimization would be too expensive to be computed, so an approximated minimization is used instead. Indeed, given an initial step length $\alpha^{(0)}$, the backtracking method tests sequentially smaller values for α until a value $\bar{\alpha}$ that satisfies the Armijo condition

$$J \left(\mathbf{C}^{(k)} + \alpha \mathbf{d} \right) \leq J \left(\mathbf{C}^{(k)} \right) + c_1 \alpha \left(\nabla J \left(\mathbf{C}^{(k)} \right), \mathbf{d} \right),$$

for a given constant c_1 , is found. Algorithm 1 sums up the complete solution method for problem 1. For further details, see for example [26].

5. Numerical results

In this section, the results for various instances of problem 1 are presented. The same set of values is used for the optimal control problem parameters throughout all the cases shown. In particular, the

Algorithm 1 Optimal control problem solution method

Let an initial guess $\mathbf{C}^{(0)}$ and two positive constants $\varepsilon_g \in \varepsilon_J$ be given.

Set $k = 0$
while $\frac{\|\mathbf{C}^{(k)} - \mathbf{C}^{(k-1)}\|_{\mathcal{C}}}{\|\mathbf{C}^{(k-1)}\|_{\mathcal{C}}} > \varepsilon_g \wedge \|\nabla J(\mathbf{C}^{(k+1)})\|_{\mathcal{G}} > \varepsilon_J$ **do**

Solve system (7) using steps 1P-5P and the current control value $\mathbf{C}^{(k)}$

Solve system (9) using steps 1A-5A and the newly computed solution of the state system

Set $\mathbf{d} = -\nabla J(\mathbf{C}^{(k)})$

Compute step length:

begin

Let an initial guess $\alpha^{(0)}$ and two constants $c_1 > 0$ and $c_2 \in (0, 1)$ be given

Solve system (7) using steps 1P-5P and $\mathbf{C}^{(k)} + \alpha^{(0)}\mathbf{d}$ as control value

Set $m = 0$

while $J(\mathbf{C}^{(k)} + \alpha^{(m)}\mathbf{d}) > J(\mathbf{C}^{(k)}) + c_1\alpha^{(m)}(\nabla J(\mathbf{C}^{(k)}), \mathbf{d})$ **do**

Set $\alpha^{(m+1)} = c_2\alpha^{(m)}$

Solve system (7) using steps 1P-5P and $\mathbf{C}^{(k)} + \alpha^{(m+1)}\mathbf{d}$ as control value

$m \leftarrow m + 1$

end while

end

Set $\mathbf{C}^{(k+1)} = \mathbf{C}^{(k)} + \alpha^{(m)}\mathbf{d}$

$k \leftarrow k + 1$

end while

values chosen for the penalization parameters in equation (8) are $\sigma_1 = 100$ and $\sigma_2 = 10^{-6}$, while the initial guess for the control function $\mathbf{C}(\mathbf{x}, t)$ is

$$\mathbf{C}^{(0)}(\mathbf{x}, t) = \begin{pmatrix} 0 \\ 0 \end{pmatrix} \quad \forall (\mathbf{x}, t) \in \Omega \times [t_0, t_f].$$

In algorithm 1, c_1 , c_2 and $\alpha^{(0)}$ are set to 0.001, 0.5 and 1, respectively, while the thresholds for the convergence check are $\varepsilon_g = \varepsilon_J = 10^{-6}$.

As for the physical parameters, the values chosen for the viscosity are $\mu_l = 1$ and $\mu_g = 0.1$, while the density is equal to $\rho_l = 10$ in the liquid and will have different values in the gas, depending on the test case. The specific gas constant is set to 300 and the temperature is 300. All the dimensional quantities are expressed in the International System of Units (SI).

With the aim of reducing the computational burden, all the numerical results of the present section have been obtained by employing an inexact version of the gradient method presented in section 4. More specifically, the adjoint system (9) has been solved by setting to zero the term $R(\varphi, \hat{\mathbf{u}})$. This choice clearly yields an approximated value for the gradient $\nabla_{\mathbf{C}} J$. Moreover, in the numerical tests, mild viscosity and density ratios are considered in order to limit the numerical issues associated with large discontinuities in the coefficients. Still, the numerical results shown in this section are paradigmatic and represent a first step towards the application of optimal control problems to two-phase compressible-incompressible flows.

5.1. Test case 1: target control reconstruction

In this first test case, a given known value is preliminarily used for \mathbf{C} in equation (7) to compute the target position of the bubbles. Then the optimal control problem is setup to drive the system towards such a desired configuration.

The initial configuration is represented in figure 3. The domain is a square with sides $L_1 = L_2 = 2$ and it was discretized using a structured triangular grid with $N = 80$ nodes on each side. The two bubbles are initially at rest in the domain, with centers in $(0.5, 0.5)$ and $(1.5, 1.5)$, radiuses $r_1 = r_2 = 0.2$ and densities $\rho_1 = 1$ and $\rho_2 = 2$, corresponding to pressures $p_1 = 90000$ and $p_2 = 180000$, respectively. The final time is $t_f = 1$ and the time step is $\Delta t = 0.05$. No gravity is considered.

The chosen target control is:

$$\mathbf{C}_t = \begin{pmatrix} 0 \\ -5 \end{pmatrix}.$$

In this case, the optimal control problem 1 is solved in the set of admissible control containing constant 2D vectors.

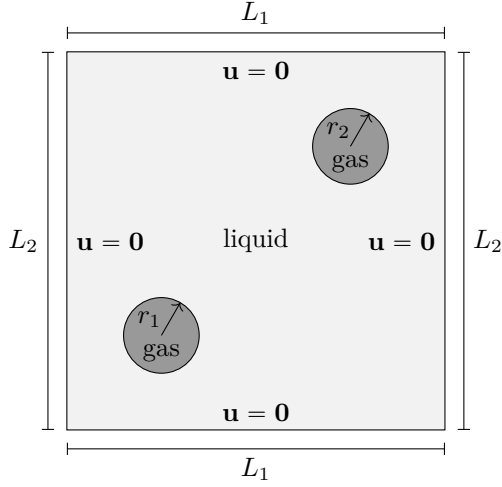


Figure 3: Test case 1, initial position of the bubbles

The history of convergence obtained by employing algorithm 1 is plotted in figure 4, while figure 5 shows the time evolution of the bubbles' position once the obtained optimal control is employed for the solution of the primal system. Such optimal control has value:

$$\mathbf{C}^* = \begin{pmatrix} 5.858 \times 10^{-5} \\ -4.9998 \end{pmatrix}.$$

First of all, let us notice that the targets are well recovered by the optimal solution, in terms of both the bubbles' position (figure 5) and the value of the control function \mathbf{C} . As for the history of convergence (figure 4), the plots for the functional value and its gradient norm show a decrease in both quantities at each minimization iteration. Finally, the figure presenting the number of backtracking iterations shows that the adopted choice for the backtracking parameters is enough to satisfy Armijo's condition.

5.2. Test case 2: controlling the final height

Figure 6 shows the initial settings for the second test case. Once again, we consider a square domain with sides $L_1 = L_2 = 2$, which was discretized using a structured triangular grid with $N = 80$ nodes on each side. The two bubbles, initially at rest, are placed in the liquid domain, with centers in $(0.5, 0.5)$ and $(1.5, 0.5)$, radii $r_1 = r_2 = 0.25$ and initial densities $\rho_1 = 1$ and $\rho_2 = 3$, corresponding to pressures $p_1 = 90000$ and $p_2 = 270000$, respectively. The final time is $t_f = 1$ and the time step is $\Delta t = 0.05$. Gravity is $\mathbf{g} = (0, -9.81)$.

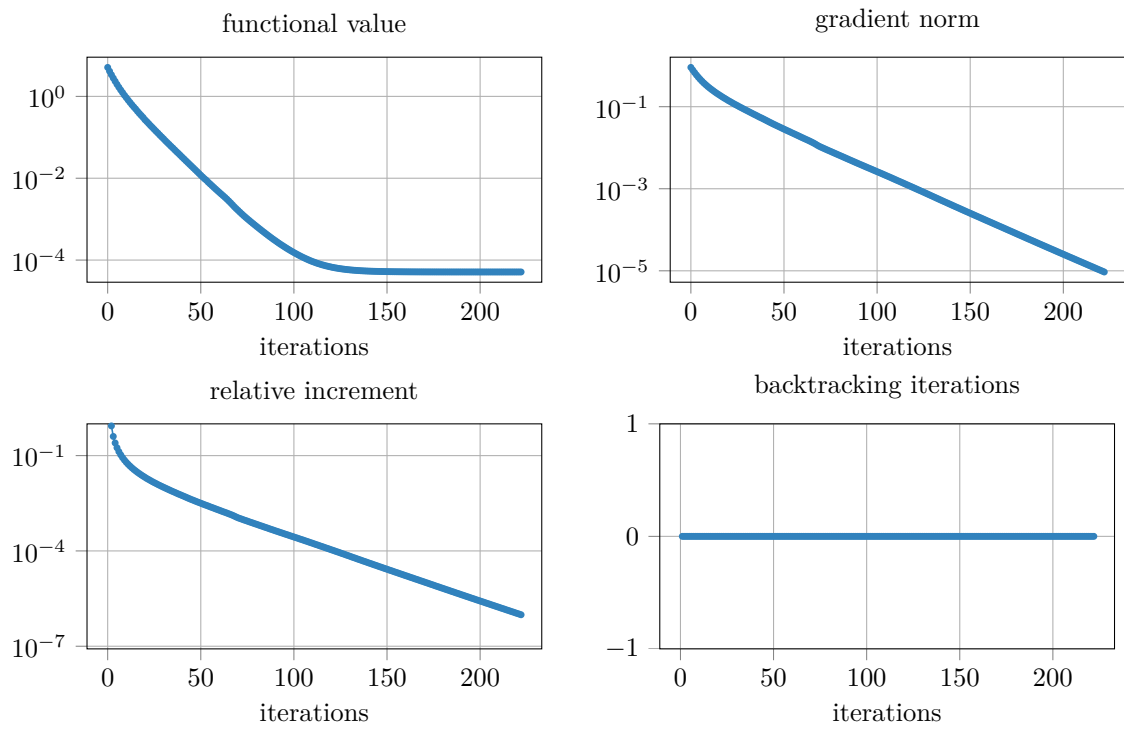


Figure 4: Test case 1, history of convergence

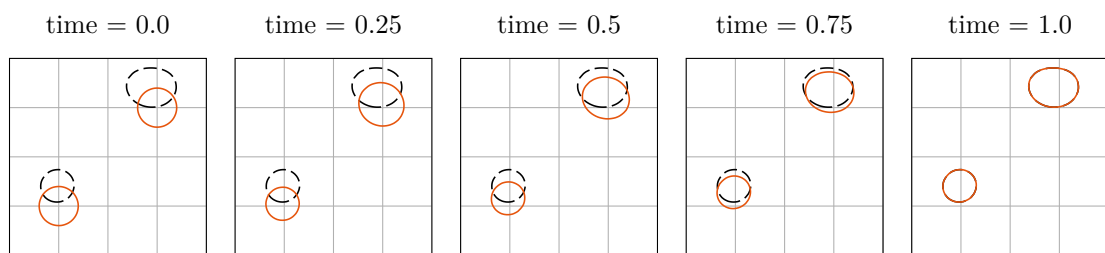


Figure 5: Test case 1, evolution of the bubbles' position employing the computed optimal control (in orange) and target position (in dashed black)

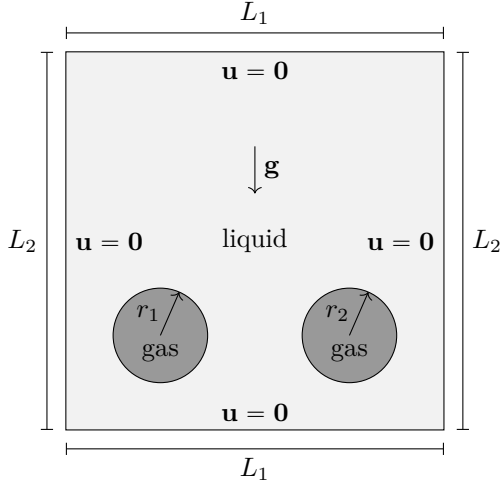


Figure 6: Test case 2, initial position of the bubbles

Having the bubbles different pressures but equal volume at the initial state, they would be pushed upwards at different speed by the buoyancy force. The aim of the solution of the optimal control problem is to prevent this phenomenon from happening, driving the bubbles to the same height instead. To do so, the target position of the two bubbles is chosen to be centered in $(0.5, 1)$ and $(1.5, 1)$, with radiuses given by

$$\begin{aligned} r_{1,f} &= \sqrt{\frac{\rho_1}{\rho_1 + \rho_2} (r_1^2 + r_2^2)} \simeq 0.1767767, \\ r_{2,f} &= \sqrt{\frac{\rho_2}{\rho_1 + \rho_2} (r_1^2 + r_2^2)} \simeq 0.3061862. \end{aligned} \quad (13)$$

Figures 7 and 8 show the history of convergence and the results of the optimal control problem, respectively.

As can be seen from the plots in the middle row of figure 8, the target is well recovered by the optimal solution. The target and computed bubbles' positions are not exactly superimposed, but are clearly much closer if compared to the respective positions of the target and the uncontrolled bubbles at final time (figure 8, top row). Furthermore, and more importantly, the obtained optimal control does indeed drive the bubbles to a position where both centers are at the same height, as desired.

From figure 7, which shows the history of convergence, we appreciate the efficacy of the gradient-type algorithm in reducing the cost functional.

5.3. Test case 3: controlling the topology

The initial configuration for the last test case is shown in figure 9. For this test case, we move to

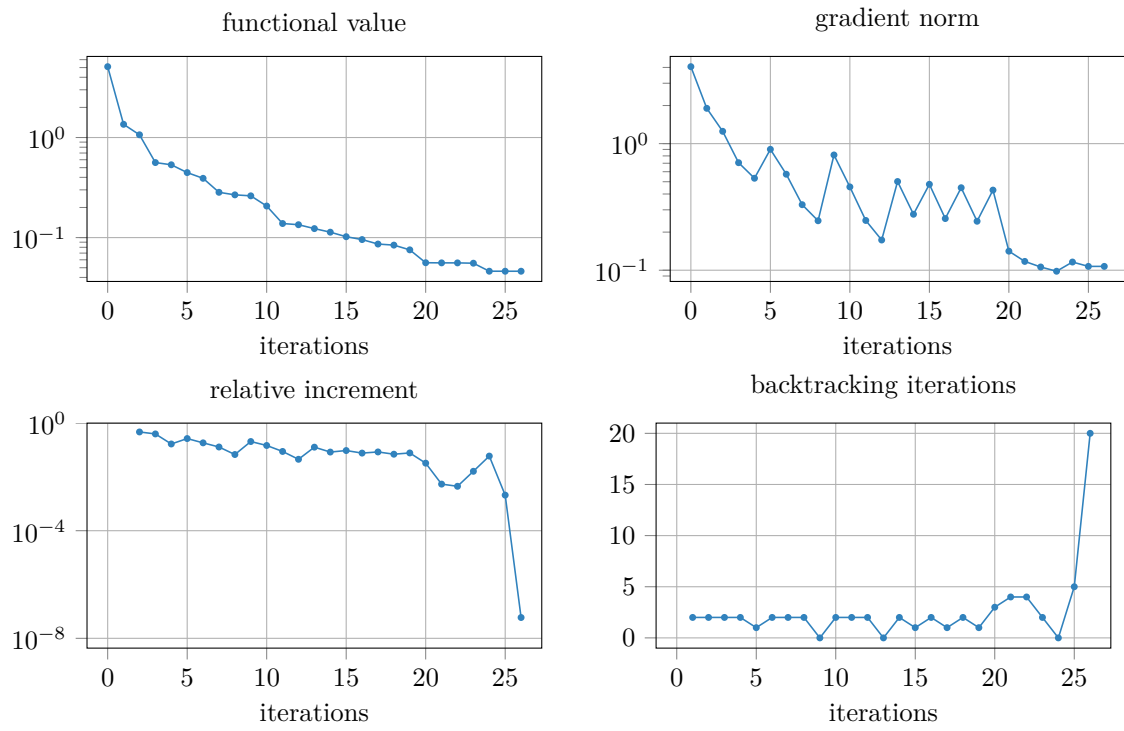


Figure 7: Test case 2, history of convergence

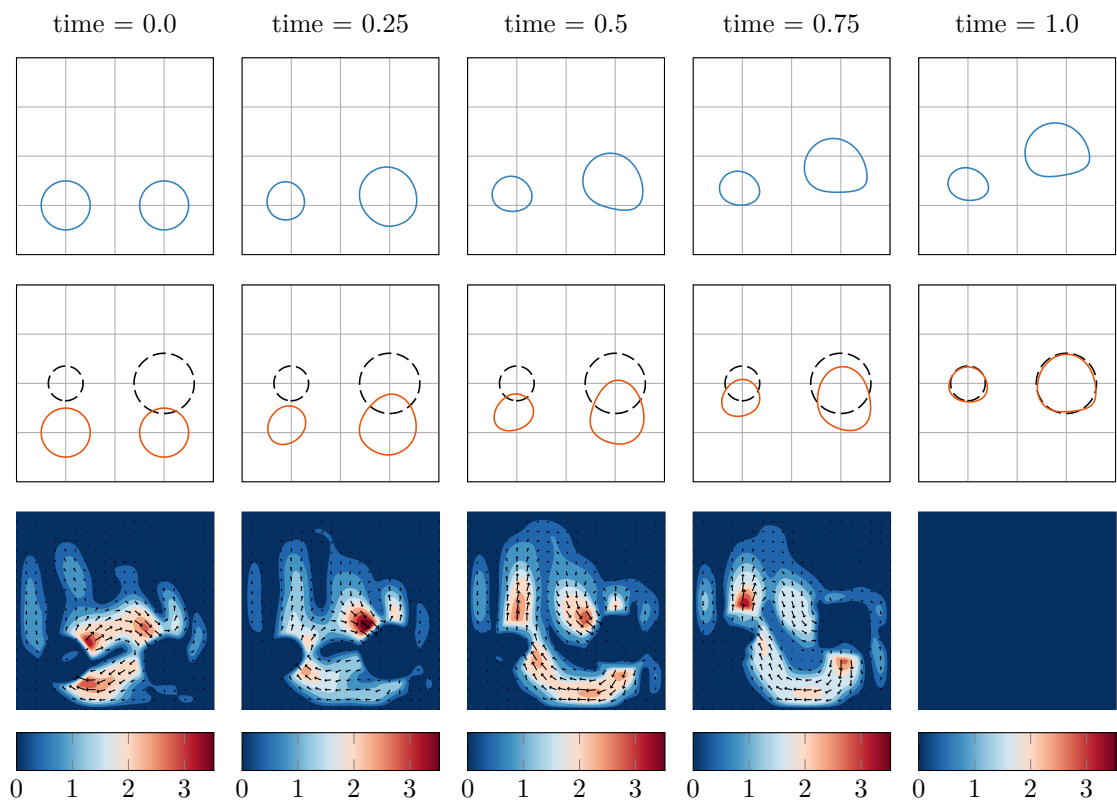


Figure 8: Test case 2, optimal control problem results. Top row: uncontrolled solution. Middle row: controlled solution (orange) and target position (dashed black). Bottom row: computed optimal control

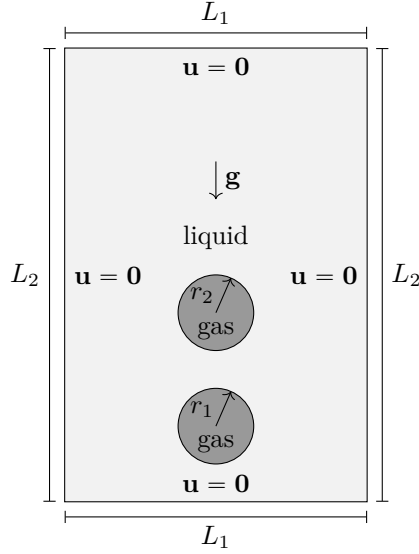


Figure 9: Test case 3, initial position of the bubbles

a rectangular domain with sides $L_1 = 2$ and $L_2 = 3$, which has been discretized using a structured triangular grid with $N_1 = 80$ nodes on L_1 and $N_2 = 120$ nodes along L_2 , so that the grid size is the same on both sides. The two bubbles have initial centers in $(1, 0.5)$ and $(1, 1.25)$ and radiuses $r_1 = r_2 = 0.25$, while the densities are set to $\rho_1 = 1$ and $\rho_2 = 3$, corresponding to pressures $p_1 = 90000$ and $p_2 = 270000$, respectively. The final time is $t_f = 1.5$ and the time step is $\Delta t = 0.05$. Gravity is $\mathbf{g} = (0, -9.81)$.

The goal of this test case is to control the topology of the bubbles. In the uncontrolled case, the higher-pressure bubble placed initially at the bottom would rise quicker than the top one, ending in a merging of the two, thus giving rise to a larger single bubble. The goal of the optimal control problem is to keep the two bubbles separated up until the end of the simulation. To this end, the target position chosen for the two bubbles has centers in $(1, 1.75)$ and $(1, 2.5)$, so that they maintain the same relative distance as in the initial state, and radiuses given by equation (13).

The history of convergence and the results of the optimal control problem are shown in figures 10 and 11, respectively.

Once again, the target is reached by the optimal solution. In particular, the goal of having two separate bubbles at the end of the simulation is accomplished. The history of convergence shows that the functional decreases along the iterations.

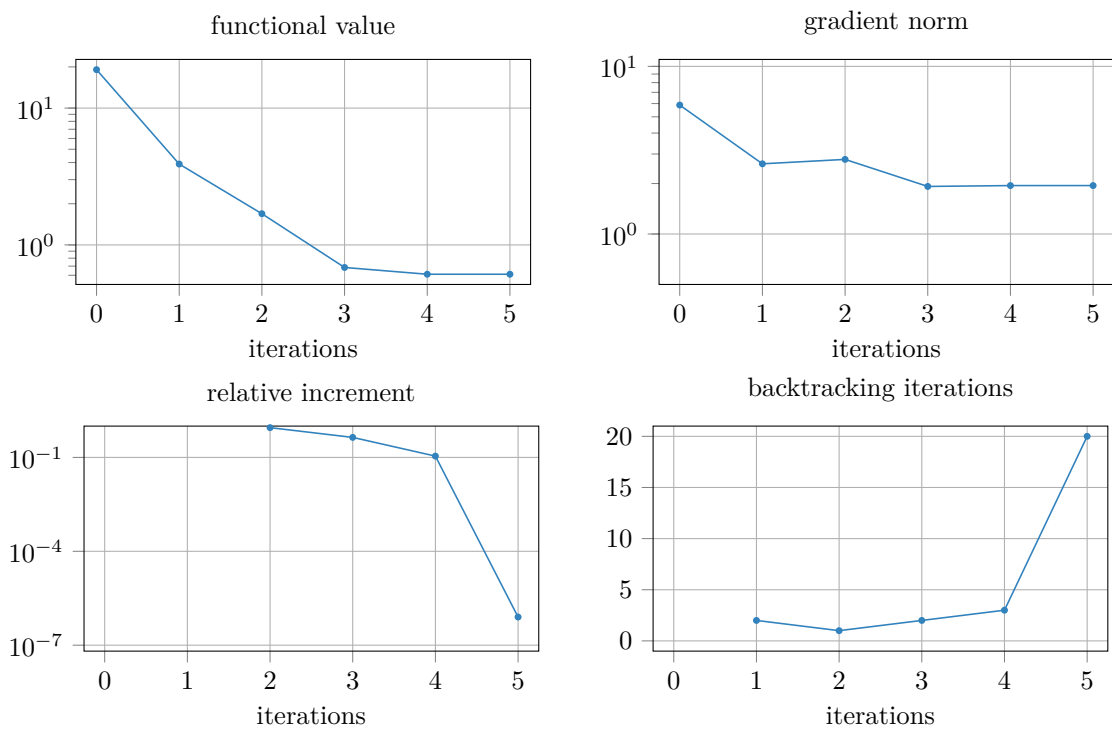


Figure 10: Test case 3, history of convergence

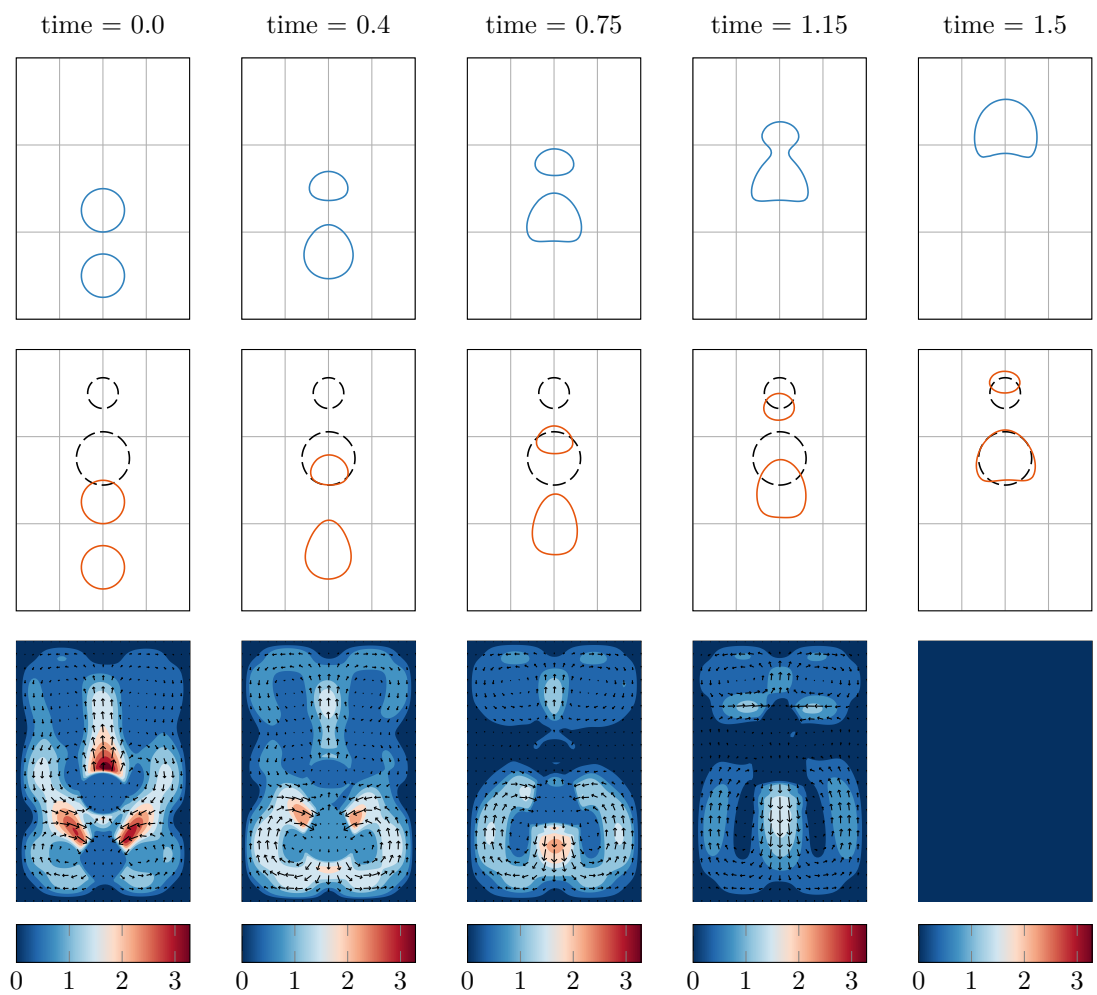


Figure 11: Test case 3, optimal control problem results. Top row: uncontrolled solution. Middle row: controlled solution (orange) and target position (dashed black). Bottom row: computed optimal control

6. Conclusions

In this work, the controllability of two-phase compressible-incompressible flows has been numerically investigated. The model introduced in [12] has been employed to govern the optimal control problem. The optimality conditions give rise to three coupled systems of equations, which have been numerically discretized to obtain a gradient-type algorithm.

Several numerical experiments were conducted, showing the efficacy of the proposed methodology and paving the way for more realistic simulations related to the production of metal foams. These test cases show that the physical system is indeed controllable, both when a specific final position of the gas bubbles and when a specific topology (or a specific number of bubbles) is required. This means that by choosing a proper forcing term in the momentum equation the system can be driven to a configuration that would not be the natural solution of the equations system, if left uncontrolled.

A possible topic for future work may be to extend this approach to use a type of control that is closer to what one would employ in an industrial framework. Indeed, a distributed volumetric force can hardly be applied consistently and precisely during the foaming process. A better choice could perhaps be to use the local temperature in the domain as the control variable. This, on the other hand, would entail the extensions to the non-isothermal case of both the physical model and the corresponding optimality conditions in the optimal control problem.

Acknowledgements

The first author would like to thank Elie Hachem for hosting his visit at CEMEF (MINES ParisTech). The authors acknowledge the partial support of INdAM-GNCS.

References

- [1] J. Banhart, *Manufacture, characterisation and application of cellular metals and metal foams*, *Progress in Materials Science* 46 (6) (2001) 559–632.
- [2] E. Repossi, R. Rosso, M. Verani, *A phase-field model for liquid–gas mixtures: mathematical modelling and discontinuous Galerkin discretization*, *Calcolo* 54 (4) (2017) 1339–1377.
- [3] M. Owkes, O. Desjardins, *A discontinuous Galerkin conservative level set scheme for interface capturing in multiphase flows*, *Journal of Computational Physics* 249 (2013) 275–302.
- [4] J. A. Sethian, P. Smereka, *Level Set Methods for Fluid Interfaces*, *Annual Review of Fluid Mechanics* 35 (1) (2003) 341–372.

- [5] C. W. Hirt, B. D. Nichols, Volume of fluid (VOF) method for the dynamics of free boundaries, *Journal of Computational Physics* 39 (1) (1981) 201–225.
- [6] R. P. Fedkiw, T. Aslam, B. Merriman, S. Osher, A Non-oscillatory Eulerian Approach to Interfaces in Multimaterial Flows (the Ghost Fluid Method), *Journal of Computational Physics* 152 (1999) 457–492.
- [7] M. Aanjaneya, S. Patkar, R. Fedkiw, A monolithic mass tracking formulation for bubbles in incompressible flow, *Journal of Computational Physics* 247 (2013) 17–61.
- [8] A. Caboussat, M. Picasso, J. Rappaz, Numerical simulation of free surface incompressible liquid flows surrounded by compressible gas, *Journal of Computational Physics* 203 (2) (2005) 626–649.
- [9] A. Caboussat, P. Clausen, J. Rappaz, Numerical simulation of two-phase flow with interface tracking by adaptive Eulerian grid subdivision, *Mathematical and Computer Modelling* 55 (3-4) (2012) 490–504.
- [10] R. Caiden, R. P. Fedkiw, C. Anderson, A Numerical Method for Two-Phase Flow Consisting of Separate Compressible and Incompressible Regions, *Journal of Computational Physics* 166 (1) (2001) 1–27.
- [11] S. Lind, P. Stansby, B. Rogers, Incompressible–compressible flows with a transient discontinuous interface using smoothed particle hydrodynamics (SPH), *Journal of Computational Physics* 309 (2016) 129–147.
- [12] M. Billaud, G. Gallice, B. Nkonga, A simple stabilized finite element method for solving two phase compressible-incompressible interface flows, *Computer Methods in Applied Mechanics and Engineering* 200 (9-12) (2011) 1272–1290.
- [13] J.-P. Caltagirone, S. Vincent, C. Caruyer, A multiphase compressible model for the simulation of multiphase flows, *Computers and Fluids* 50 (1) (2011) 24–34.
- [14] V. Daru, P. Le Quéré, M.-C. Duluc, O. Le Maître, A numerical method for the simulation of low Mach number liquid–gas flows, *Journal of Computational Physics* 229 (23) (2010) 8844–8867.
- [15] S. Paolucci, On the filtering of sound from the Navier Stokes equations, Tech. Rep. Report SAND-82-8257, SANDIA National Laboratory (1982).
- [16] T. Alazard, Low Mach Number Limit of the Full Navier-Stokes Equations, *Archive for Rational Mechanics and Analysis* 180 (1) (2005) 1–73.

- [17] E. Hachem, M. Khalloufi, J. Bruchon, R. Valette, Y. Mesri, Unified adaptive Variational MultiScale method for two phase compressible-incompressible flows, *Computer Methods in Applied Mechanics and Engineering* 308 (2016) 238–255.
- [18] D. Colton, R. Ewing, W. Rundell, *Inverse problems in partial differential equations*, Vol. 42, Siam, 1990.
- [19] J. L. Lions, *Optimal control of systems governed by partial differential equations*, Springer, 1971.
- [20] F. Tröltzsch, *Optimal Control Of Partial Differential Equations*, Vol. 112, American Mathematical Society, 2010.
- [21] M. D. Gunzburger, *Perspectives in Flow Control and Optimization*, Vol. 5, SIAM, 2003.
- [22] N. Parolini, *Computational fluid dynamics for naval engineering problems*, Ph.D. thesis, École Polytechnique Fédérale de Lausanne (2004).
- [23] M. Tamellini, *Two-phase compressible-incompressible problems: numerical methods and optimal control*, Phd thesis (in preparation), Politecnico di Milano.
- [24] A. Quarteroni, A. Valli, *Numerical Approximation of Partial Differential Equations*, Springer, 1996.
- [25] D. A. Di Pietro, S. Lo Forte, N. Parolini, Mass preserving finite element implementations of the level set method, *Applied Numerical Mathematics* 56 (9) (2006) 1179–1195.
- [26] S. J. Wright, J. Nocedal, *Numerical optimization*, Vol. 35, Springer, 1999.

MOX Technical Reports, last issues

Dipartimento di Matematica
Politecnico di Milano, Via Bonardi 9 - 20133 Milano (Italy)

- 64/2017** Fumagalli, I.; Parolini, N.; Verani, M.
Optimal control in ink-jet printing via instantaneous control
- 65/2017** Regazzoni, F.; Parolini, N.; Verani M.
Topology optimization of multiple anisotropic materials, with application to self-assembling diblock copolymers
- 62/2017** Barbarotta, L.; Rossi, S.; Dede', L.; Quarteroni, A.
A Transmurally Heterogeneous Orthotropic Activation Model for Ventricular Contraction and its Numerical Validation
- 63/2017** Masci, C.; Paganoni, A.M.; Ieva, F.
Non-parametric mixed-effects models for unsupervised classification of Italian schools
- 61/2017** Vadacca, L.; Colciago, C. M.; Micheletti, S.; Scotti, A.
Three-dimensional fault representation by interface and solid elements: effects of the anisotropy of the fault zone permeability on the timing of triggered earthquakes
- 60/2017** Bonaldi, F.; Di Pietro, D. A.; Geymonat, G.; Krasucki, F.
A Hybrid High-Order method for Kirchhoff-Love plate bending problems
- 59/2017** Grujic, O.; Menafoglio, A.; Guang, Y.; Caers, J.
Cokriging for multivariate Hilbert space valued random fields. Application to multifidelity computer code emulation
- 58/2017** Landajuela, M.; Vergara, C.; Gerbi, A.; Dede', L.; Formaggia, L.; Quarteroni, A.
Numerical approximation of the electromechanical coupling in the left ventricle with inclusion of the Purkinje network
- 56/2017** Alberti, G. S.; Santacesaria, M.
Infinite dimensional compressed sensing from anisotropic measurements
- 57/2017** Ballarin, F.; D'Amario, A.; Perotto, S.; Rozza, G.
A POD-Selective Inverse Distance Weighting method for fast parametrized shape morphing